Journal of Chromatography, 282 (1983) 193–209
Elsevier Science Publishers B.V., Amsterdam — Printed in The Netherlands

CHROMSYMP. 161

LIQUID CHROMATOGRAPHIC DETECTION OF CARDIAC GLYCOSIDES AND SACCHARIDES BASED ON THE PHOTOREDUCTION OF ANTHRAQUINONE-2,6-DISULFONATE

M. S. GANDELMAN* and J. W. BIRKS
Department of Chemistry and Cooperative Institute for Research in Environmental Sciences (CIRES), University of Colorado, Boulder, CO 80309 (U.S.A.)
and
U. A. Th. BRINKMAN and R. W. FREI*
Department of Analytical Chemistry, Free University, De Boelelaan 1083, 1081 HV Amsterdam (The Netherlands)

SUMMARY

The photoreduction fluorescence detector functions by monitoring the change in fluorescence accompanying the photoreduction of anthraquinone-2,6-disulfonate to dihydroxyanthracene-2,6-disulfonate by alcohols, aldehydes, ethers, and saccharides. Since the photoreduction of anthraquinone only requires the anthraquinone and not the analyte (alcohol aldehyde, etc.) to absorb light, the detector can be employed to determine compounds which have extremely low UV–visible extinction coefficients. In this paper we present detailed optimization studies on the photochemistry involved in this detection scheme and demonstrate this detector for the determination of cardiac glycosides and common food saccharides in relevant samples. Detection limits for the the cardiac glycosides are in the low picomole range, whereas the saccharides can be determined in the low nanomole range. The detector exhibits a linear response for diginatin in the range 50–500 ng; the reproducibility was calculated to be 6.0% RSD.

INTRODUCTION

Over the last decade, liquid chromatography (LC), especially high-performance liquid chromatography (HPLC), has been the fastest growing analytical technique. This rapid rise in popularity is due to the almost universal chromatographic applicability of LC; for instance, many polar and most ionic compounds are not volatile enough to be separated by gas chromatography (GC) without sample pretreatment, whereas separation by LC can be rather trivial for the underivatized compounds. However, the state of the art in LC detectors is still limited by the lack of

* Future address: University of Connecticut, School of Medicine, Farmington, CT 06032, U.S.A.

0021-9673/83/$03.00

widely applicable, sensitive and selective detectors. The refractive index (RI) detector, a universal detector for LC, has rather poor sensitivity and stringent operating conditions. The ultraviolet absorption (UV) detector, the most popular LC detector, has little selectivity and in general only moderate sensitivity. Allthough fluorescence and electrochemical detectors have adequate sensitivity and selectivity, their applicability is severely limited, since only a relatively small group of compounds exhibits native fluorescence or electrochemical activity. Consequently, the development of new, sensitive and selective HPLC detectors is a must, if LC is to keep pace with the demands of analytical chemistry. In particular, functional group- and heteroatom-selective detectors are a hope for the future.

Post-column reaction detectors recently have contributed successfully to LC detection, since these detectors have in many cases demonstrated the selectivity and sensitivity needed for modern analyses. A few thorough reviews have been written on this subject[1–4]. In this study, we have examined a special type of post-column reaction detector, namely a photochemical reaction detector. Photochemical reaction detectors have recently been reviewed by Birks and Frei[5]. These detectors have some advantages over the thermochemical post-column reaction detectors. First, the addition of photons as a chemical reagent requires no mixing device, and consequently no chemical dilution of the analyte will occur. Second, since many photochemical reactions proceed via free radical intermediates, the reaction kinetics are often quite rapid so that only short residence times are required in the photochemical reactor. Finally, the use of a monochromator or an optical filter to limit the spectral output of the photochemical source may provide additional selectivity in the determination.

Generally, two types of photochemical reaction have been employed in post-column reaction detectors. Photolytic reactions have been used to produce a particular product, usually an ion, which can be subsequently detected, *e.g.* by conductivity detectors. Fluorophor-producing or -enhancing photochemical reactions make up the second and largest group of photochemical reactions. Although this group of reactions is rather varied, the photochemical reactions usually increase the rigidity or the aromatic character of the molecule. However, some reactions may improve the fluorescence efficiency of a molecule by simply changing the oxidation state of a particular heteroatom within the molecule.

Iwaoka and Tannenbaum[6] reported the first use of a post-column photochemical reactor in which N-nitroso compounds were selectively detected in food products in the range 10–100 ng/g. This was done by photolyzing the N-nitroso compounds to produce nitrite, which was subsequently determined colorimetrically by the Griess reaction. Similarly, the photoconductivity detector, invented by Hall and Rodgers[7] and marketed by Tracor, functions by photolytically decomposing halogen-, nitrogen- and sulfur-containing compounds to produce ionic products. These ions are then determined by a conductivity detector. Reported detection limits for some compounds are in the low picogram range. Recently Gandelman and Birks[8] have demonstrated the use of chemiluminescence, combined with photochemical reaction detectors. In their detection system alcohols, aldehydes, ethers, and saccharides, react in a sensitized photo-oxygenation mechanism to produce hydrogen peroxide, which is subsequently determined by the luminol chemiluminescence reaction.

The fluorophor production or enhancement by photochemical reactions has found its greatest use in the fields of pharmaceutical and forensic analyses. The ap-

plication of this type of photochemical reaction was first demonstrated by Twitchett *et al.*[9] for the determination of subnanogram amounts of cannabinol in urine. Cannabinol, a non-fluorescent compound, undergoes a ring opening, hydrogen transfer, dehydrogenation, and ring closure to produce a hydroxyphenanthrene, a highly fluorescent molecule[10]. Harman and Blackman[11] photocyclized clomiphene, a stilbene ovulatory stimulant, to a phenanthrene, also a highly fluorescent product, and reported a detection limit of 60 pg for clomiphene. Similarly, Rhys Williams *et al.*[12] have photocyclized another stilbene type of compound, diethylstilbestrol (DES), which is an estrogenic compound, and were able to determine 1 ng/g of DES in human urine. Scholten *et al.*[13–14] and Brinkman *et al.*[15] have photochemically oxidized various phenothiazines to increase the fluorescence efficiency of these compounds, and detection limits of *ca.* 40–100 pg were obtained[15]. Additionally, the same group[13–15] and Uihlein and Schwab[16] have photochemically transformed some non-fluorescent benzodiazepine tranquilizers and a few of their metabolic products (clobazam, desmethylclobazam and demoxepam) into their fluorescent quinazolinone derivatives. Detection limits varied, depending on the type of photochemical reactor and fluorometer; detection limits of 100 pg for demoxepam[15], 70 pg for clobazam and 100 pg for desmethylclobazam are reported[13]. Lefevere *et al.*[17] photoreduced vitamin K_1, a non-fluorescent naphthoquinone, to produce the naphthoquinol, a highly fluorescent product. Detection limits of *ca.* 60 pg were reported. Finally, Scholten *et al.*[18] have discussed the combination of photochemical reactors with solvent segmentation, which allows extended residence times within the photochemical reactor.

The post-column photochemical reaction demonstrated in this study has been previously described for the determination of aliphatic alcohols, aldehydes, and ethers by Gandelman and Birks[19]. This type of detector system functions differently from the previously reviewed photochemical reactors. All the photochemical reactions previously discussed, except for the photo-oxygenation chemiluminescence detector[8], require the analyte to absorb the UV light of the photochemical source and undergo some type of photochemical transformation. Furthermore, these detectors are only sensitive to a narrow group of analytes. In our system, the photoreduction fluorescence (PRF) detector, a photochemical reagent (anthraquinone-2,6-disulfonate) absorbs the UV radiation from the photochemical source and reacts with the analytes to produce a fluorescent product (dihydroxyanthracene-2,6-disulfonate). Consequently, the analytes need not absorb any UV radiation to produce a fluorescent molecule. In addition, the detector is sensitive to several organic functional groups, and thus the detection system responds to a wide variety of compounds. For this study, we chose cardiac glycosides and saccharides as model compounds to demonstrate the capabilities of the PRF detector. Both classes of compounds are difficult to determine by LC and GC. Since these compounds are involatile owing to their high polarity, separation by GC is impossible without prior derivatization. The separation is not difficult in LC; however, the sensitivity of conventional LC detectors toward these compounds, especially the saccharides, is poor.

THEORETICAL

The PRF detection scheme is based on the dramatic change in the fluorescence

quantum yield (Φ_F) accompanying the photoreduction of anthraquinone-2,6-disulfonate (AQDS) to 9,10-dihydroxyanthracene-2,6-disulfonate (AQH_2DS). The photoreduction only occurs in the presence of hydrogen-atom-donating substrates (*e.g.* alcohols, aldehydes, allylic and benzylic hydrocarbons, amines, ethers and saccharides) which contain a weak C–H bond[20]. Our work has concentrated on the detection of oxygen-containing compounds. The oxygen atoms in these molecules inductively weaken the C–H bonds of α-hydrogens. By conducting the photoreduction in solvents inert to hydrogen abstraction (acetonitrile and water) trace amounts of these hydrogen-atom-donating substrates can be determined by the increase in fluorescence accompanying the photoreduction of AQDS to AQH_2DS.

This type of photoreduction is one of the most thoroughly studied reactions in organic photochemistry[21–28]. The sequence of reactions begins with the absorption of light by the AQDS. AQDS has two major absorption bands, the first near 360 nm, which represents the $n \rightarrow \pi^*$ transition, while the second absorption band is from the $\pi \rightarrow \pi^*$ transition and occurs near 250 nm. The quantum yield for photoreduction is independent of the excitation wavelength, since the internal conversion to the lowest excited singlet is so rapid that the absorption of a photon of any energy rapidly produces the AQDS in $S_1(n, \pi^*)$. From $S_1(n, \pi^*)$ the molecule undergoes intersystem crossing to the lowest triplet state (T_1), which also has a molecular configuration of (n, π^*). The $T_1(n, \pi^*)$ state is biradical in character and undergoes reactions similar to alkoxy radicals[20]. The photochemical reactions of the excited triplet state must compete with other photophysical processes which deactivate T_1. Unfortunately, the efficiency of the photochemical processes (*ca.* 10^{-7}%) is rather poor at analyte concentrations of interest (*ca.* 10^{-3} *M*). At such low analyte concentrations the non-radiative intersystem crossing process $T_1 \rightarrow S_0$ dominates the depopulation of T_1. In the presence of a hydrogen-atom-donating substrate the $T_1(n, \pi^*)$ state of AQDS will abstract a hydrogen atom from the carbon atom α to the heteroatom, and yield two radical products, the semiquinone and α-hydroxyalkyl radical (if the substrate is an alcohol). This hydrogen abstraction is the rate-limiting step for the photoreduction of AQDS. The two radicals undergo a series of reactions which finally yield the reduced species AQH_2DS. This reaction scheme is described in Fig. 1[24].

The reduced form of anthraquinone, dihydroxyanthracene, is an extremely fluorescent molecule[29], with a Φ_F of *ca.* 0.7, whereas anthraquinone has a Φ_F of less than 10^{-5}. This vast difference in photophysical properties of the two molecules is caused by differences in their electronic structures. The extremely low Φ_F of anthraquinone and many other carbonyl compounds is caused by the inability of the flu-

$$Q + h\nu \longrightarrow Q^* \text{ (singlet, S)}$$

$$Q^*(S) \longrightarrow Q^* \text{ (triplet, T)}$$

$$Q^*(T) + CH_3CH_2OH \longrightarrow QH\cdot + CH_3\dot{C}HOH$$

$$CH_3\dot{C}HOH + Q \longrightarrow QH\cdot + CH_3CHO$$

$$2QH\cdot \longrightarrow Q + QH_2$$

Fig. 1. Probable mechanism for photoreduction of anthraquinone-2,6-disulfonate by 2-propanol. Q is anthraquinone-2,6-disulfonate; QH· is the semiquinone radical: and QH_2 is dihydroxyanthracene-2,6-disulfonate.

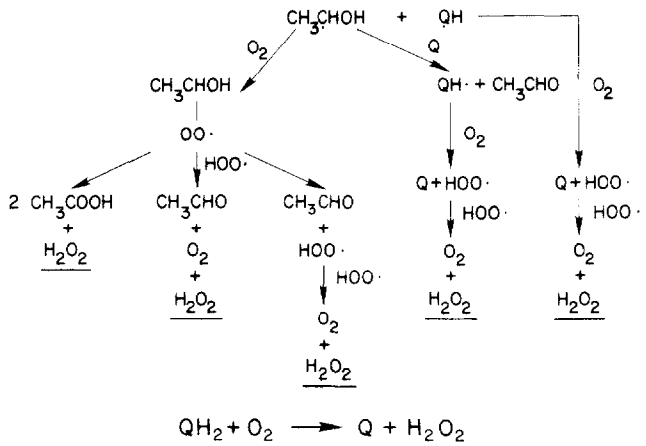

Fig. 2. Reactions of α-hydroxyethyl radical, semiquinone radical, and dihydroxyanthracene-2,6-disulfonate with O_2. Q is anthraquinone-2,6-disulfonate, QH· is the semiquinone radical, and QH_2 is dihydroxyanthracene-2,6-disulfonate.

orescence to compete with the rapid intersystem crossing from S_1 to T_1. This rapid intersystem crossing is caused by the proximity in energy of the $S_1(n, \pi^*)$ and $T_1(n, \pi^*)$ states[20]. In anthraquinone this separation is *ca.* 4 kcal mol^{-1}. In other words, the depopulation of the excited state in anthraquinone proceeds through the T_1 state by a non-radiative decay rather than by fluorescence from S_1. In contrast, since the dihydroxyanthracene does not contain a carbonyl group, the molecule does not have a low-lying $S_1(n, \pi^*)$ state, and there exists a much larger singlet–triplet energy gap in comparison with AQDS. This larger gap causes much slower intersystem crossing, and thus the fluorescence can compete with the intersystem crossing. In other words, *ca.* 70% of the excited singlet state molecules are deactivated by fluorescence emission in dihydroxyanthracene, while the vast majority of the excited state anthraquinone molecules are deactivated by intersystem crossing to T_1.

The photoreduction reaction mechanism previously mentioned is quite sensitive to oxygen, since oxygen reacts with the photochemically generated radicals[30–33] and dihydroxyanthracene, causing a branching of the desired reaction mechanism away from AQH_2DS. These additional reactions with oxygen are shown in Fig. 2. The semiquinone radical and the α-hydroxyalkyl radical (in the photoreduction of an alcohol) react with oxygen at diffusion-limited rates to produce hydrogen peroxide, the oxidized form of the alcohol (aldehyde or ketone) and AQDS. Similarly, oxygen reacts with dihydroxyanthracene to produce hydrogen peroxide and anthraquinone. The quenching effect of oxygen on the triplet excited state of AQDS is rather small, as the lifetime of the triplet is short, and even at diffusion-limited rates for oxygen quenching, the effect is almost insignificant. This fact is demonstrated by the use of AQDS as a sensitizer for photo-oxygenation reactions which occur readily in solutions saturated with air[30–32]. However, the exclusion of oxygen is essential to the photoreduction of anthraquinone, since both the radicals and dihydroxyanthracene are oxygen-sensitive. Any residual oxygen will cause a decrease in the chemical yield of AQH_2DS.

EXPERIMENTAL

Reagents

Anthraquinone-2,6-disulfonate, disodium salt (Aldrich, Milwaukee, WI, U.S.A.) was recrystallized from boiling water and washed with HPLC grade acetonitrile (Merck or Fisher). A stock solution containing 2.5 g of AQDS per liter of water ($6.05 \cdot 10^{-3}$ *M*) was made up and stored in a brown glass bottle. All acetonitrile used in the HPLC mobile phase was HPLC grade (Merck or Fisher).

Chromatographic apparatus

Three separate systems were used for chromatography. The first consisted of an Altex 100A high-pressure pump, a Valco Model C6U injector with a 15-μl loop and either a C_8 column (250 × 4.6 mm I.D.) with 10-μm particle diameter, packed with Merck LiChrosorb RP-8, or a C_{18} column (150 × 4.6 mm I.D.) with 5-μm particle diameter, packed with Merck LiChrosorb RP-18. The second system contained an Altex 110A pump, a Rheodyne 7120 injector with a 20-μl loop and an Alltech C_{18} column (250 × 4.6 mm I.D.) with 10-μm particle diameter. The third system entailed an Altex 110A high-pressure pump, a Waters 6000A high-pressure pump, a Rheodyne Model 7120 injector with a 20-μl loop, an Alltech C_{18} column (250 × 4.6 mm I.D.) with 10-μm particle diameter, an Alltech amino column (250 × 4.6 mm I.D.) with 10-μm particle diameter, and a Valco low-dead-volume mixing tee. All PTFE connections prior to the fluorometer were removed from each chromatographic system since PTFE is permeable to oxygen.

Photochemical reactors

Four photochemical reactors were tested in this study. Photochemical reactors I and II each contained a 200-W high-pressure Hg–Xe arc lamp (Hanovia model 901-B1), housed in a previously described apparatus[17]. The PTFE capillary (Omnifit, Biolab, Cambridge, U.K.) was coiled around a quartz cylinder (8-cm diameter) and immersed within a watertight cylindrical chamber through which water was circulated as a coolant. Reactor I contained 1 m of the PTFE capillary, 0.33 mm I.D. × 0.70 mm O.D., whereas reactor II consisted of only 20 cm of the same PTFE capillary. The front face of the watertight cylindrical chamber was made of quartz (6-cm diameter), and a thin piece of sheet aluminium (0.5-mm thickness) was coiled on the inside of the outer cylindrical face to increase the photon flux of the lamp by reflection.

Reactors III and IV employed a 8-W fluorescent "black lamp" (Sylvania Model E 8TS IBLB). The reaction cell in Model III (1 m of 6.4 mm O.D. × 0.45 mm I.D. Pyrex) was coiled around the fluorescent-lamp tube. Reactor IV entailed a 12.5-m knitted PTFE reactor coil. The PTFE capillary (previously described for photochemical reactors I and II) was knitted into a cylinder and slid over a 26 cm × 2 cm O.D. pyrex sleeve which then was placed over the fluorescent lamp tube. Two O-rings were placed between the lamp and the Pyrex sleeve. The Pyrex sleeve and O-ring assembly were employed to avoid overheating of the PTFE capillary. In addition, reactor IV was placed within a nitrogen-flushed Plexiglass housing to avoid any oxygen diffusion through the PTFE capillary. In reactors I and II, the PTFE reaction coils were surrounded by cooling water and the metal-to-PTFE junctions

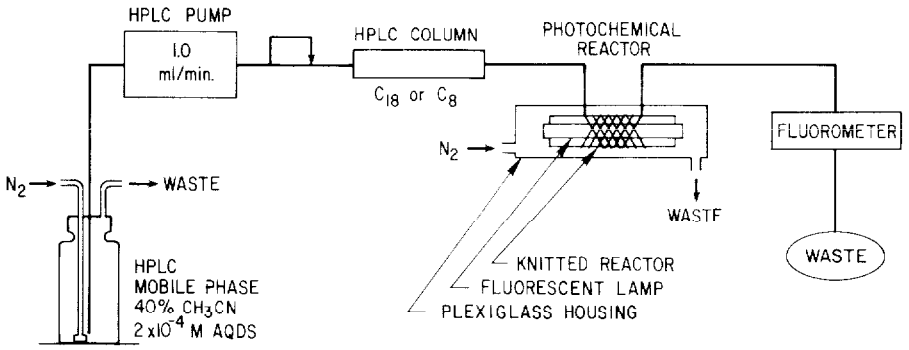

Fig. 3. Schematic diagram of the single-pump detection scheme.

were made within the watertight housing. Likewise, in reactor IV the PTFE–metal junctions were made within the nitrogen-purged housing.

Detection schemes

Two detection schemes were employed in this study. Each detection scheme can be divided into two functional units, the photochemical reactor and the fluorometer (Schoefel FS-970 or Kontron Model 100). The first scheme (Fig. 3) subsequently referred to as the single-pump scheme, involved using only one high-pressure pump and adding the photochemical reagent to the mobile phase reservoir. Consequently, the AQDS was pumped throughout the entire system (injector, analytical column, photochemical reactor, and fluorometer). The second scheme (Fig. 4) required the use of two pumps and two columns. The second pump (Waters 6000A) was used to add the photochemical reagent via a mixing tee after the amino column. The reservoir of the pump was wrapped with heating tape in order to reduce the

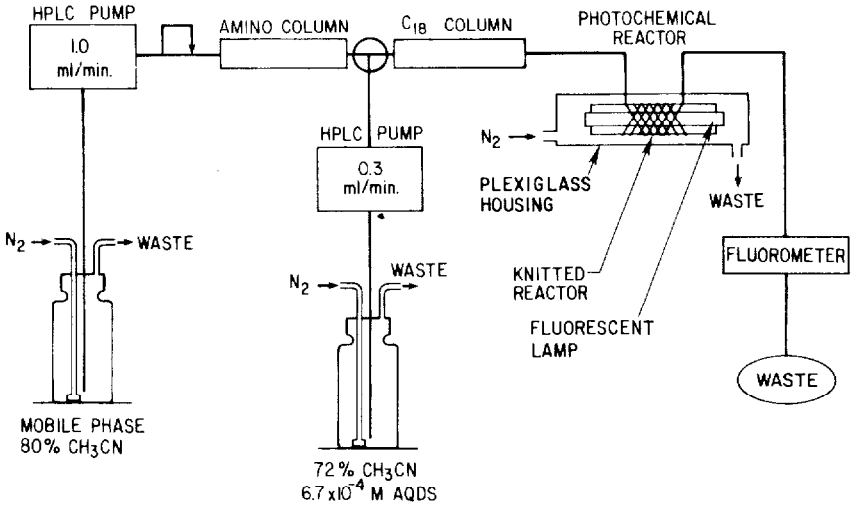

Fig. 4. Schematic diagram of the dual-pump detection scheme.

amount of dissolved nitrogen in the solution, since the low-dead-volume pistons of this pump had considerable difficulty in clearing any nitrogen bubbles. The C_{18} column was placed after the mixing tee to suppress noise due to flow pulsation. This scheme will be referred to as the dual-pump scheme.

For the Kontron fluorometer the optimal wavelength for excitation was 400 nm and that for emission was 525 nm. A filter limiting emission wavelengths to greater than 475 nm was used with the Schoefel fluorometer, and the optimal excitation wavelength was 275 nm.

Photochemical optimization measurements

The photochemical optimization measurements were made by injecting 15 μl of a 0.01% solution of the cardiac glycoside, diginatin. In addition, all optimization measurements were made by using the single-pump configuration with the C_{18} column and the Kontron fluorometer. The residence time within the reactor was varied by adjusting the flow-rate of the pump. The volumes of the reactors were determined by measuring the elution volume for a 15-μl injection of a 10^{-4} *M* solution of salicylic acid with the reactor in place and subtracting the elution volume obtained with the reactor removed.

The signal/noise (S/N) optimizations were based on peak height and peak-to-peak noise measurements, whereas the relative chemical yields of AQH_2DS were determined from peak areas by the triangulation method.

RESULTS AND DISCUSSION

Optimization of photochemistry

Three experiments were performed in order to obtain information about the kinetics of the AQDS photoreduction. For each of these experiments, a parameter of the photochemistry [either S/N, signal area (S_{area}) or background signal (S_{bg})] was plotted against residence time in the photochemical reactor for various concentrations of AQDS.

The background signal, possibly due to the photosolvation effect[29,34,35] shown in Fig. 5, is always observed in the PRF detection scheme. This background photochemical reaction is a complex function of AQDS concentration, photon flux, residence time in the photochemical reactor, and the amount of oxygen present in the solution. Two important aspects of this background reaction should be noted. First, the background reaction decreases the amount of residual oxygen present in solution by producing hydrogen peroxide in a photo-oxygenation reaction shown in Fig. 2[31].

$$Q + h\nu \longrightarrow Q^*\{\text{singlet, S}\}$$

$$Q^*(S) \longrightarrow Q^*(\text{triplet, T})$$

$$Q^*(T) + H_2O \rightleftharpoons (Q \cdot H_2O)$$

$$(Q \cdot H_2O) + Q \longrightarrow QOH\cdot + QH\cdot$$

$$2\,QH\cdot \longrightarrow Q + \underline{QH_2}$$

Fig. 5. Probable mechanism for background reaction (photosolvation). Q is anthraquinone-2,6-disulfonate, QH· is the semiquinone radical, and QH_2 is dihydroxyanthracene-2,6-disulfonate.

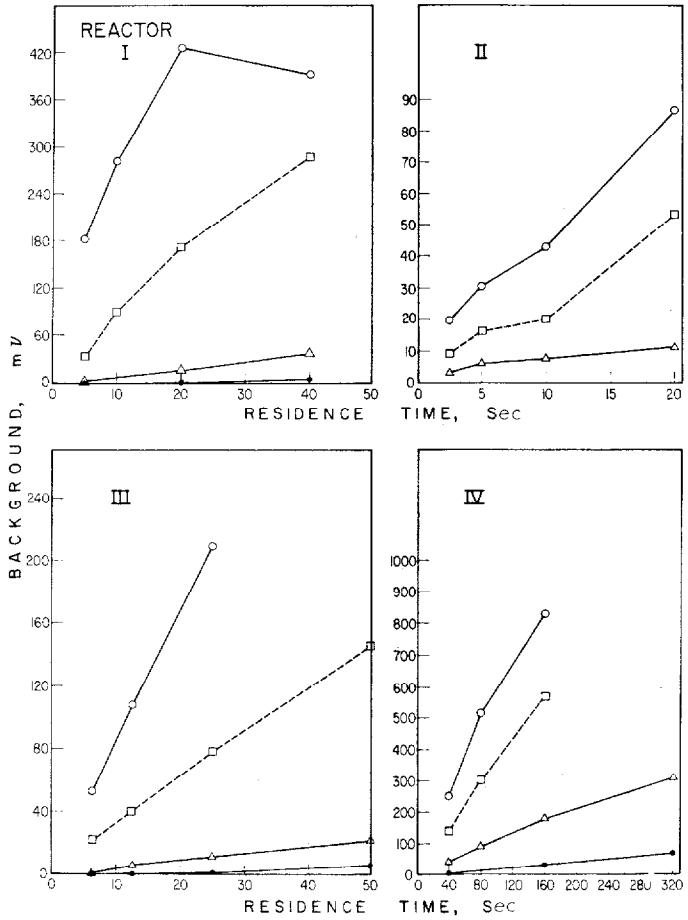

Fig. 6. Variation of the background signal with residence time in the photochemical reactors at various anthraquinone-2,6-disulfonate concentrations. Single-pump detection scheme, C_8 column, Kontron fluorometer. ○, $1.20 \cdot 10^{-3}$ *M*; □, $6.00 \cdot 10^{-4}$ *M*; △, $2.00 \cdot 10^{-4}$ *M*; ●, $4.00 \cdot 10^{-5}$ *M* anthraquinone-2,6-disulfonate.

Thus, the solutions with larger S_{bg} become lower in residual oxygen owing to the greater extent of the background reaction. Second, the noise of the system is due to the pump modulation of the background, and this noise limits the amount of analyte that can be detected. Fig. 6 shows S_{bg} for reactors I, II, III and IV, respectively. In all cases, S_{bg} rises with increasing residence time, and all the curves (each one representing a different concentration of AQDS) fall in a sequential order, which demonstrates a proportionality between S_{bg} and AQDS concentration.

The plots of S_{area} *versus* residence time shown in Fig. 7 reveal the kinetics of the photoreduction of AQDS in the presence of an analyte (diginatin), but do not address the problem of background signal. For reactor I (200-W Hg–Xe lamp, 1-mm PTFE capillary) it was observed that for the $1.21 \cdot 10^{-3}$ *M* and $6.06 \cdot 10^{-4}$ *M* AQDS concentrations the signals are larger at shorter residence times and decay sharply as the residence time increases. This is probably due to the photodegradation of the

dihydroxyanthracene to non-fluorescent products (possibly polymers) with increasing residence time. The lower concentrations of AQDS gave no signal, and this result is probably due to two concerted effects. First, the solutions are higher in residual oxygen, since the low AQDS concentrations produce less S_{bg}, and a larger proportion of residual oxygen is left unchanged. Second, the lower AQDS sensitizer concentrations produce less AQH_2DS for the same concentration of analyte compared with the higher AQDS concentrations. Since higher concentrations of residual oxygen are present, the AQH_2DS produced may be oxidized by the residual oxygen back to AQDS, and thus no signal is detected. Reactor II (200-W Hg–Xe lamp, 20-cm PTFE capillary) demonstrates behavior similar to that of reactor I with the exception that the absolute signal values are somewhat lower. Both reactors have an optimum residence time of *ca.* 10 sec.

For reactor III (8-W black lamp, 1-m Pyrex capillary) the signals continually

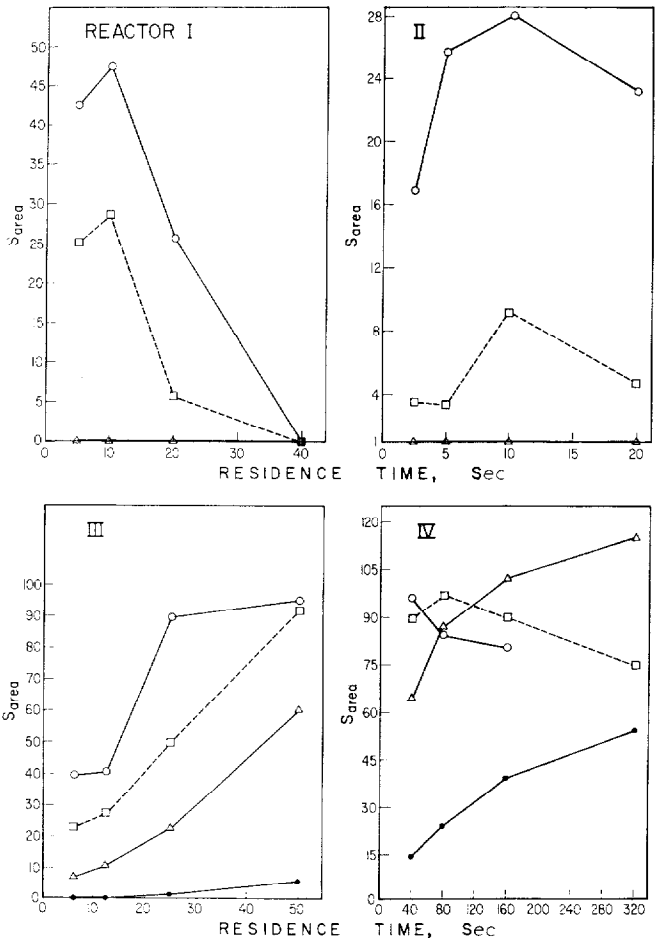

Fig. 7. Signal area *vs.* residence time in the photochemical reactor at various anthraquinone-2,6-disulfonate concentrations. Single-pump detection scheme, C_8 column, Kontron fluorometer. ○, $1.20 \cdot 10^{-3}$ *M*; □, $6.00 \cdot 10^{-4}$ *M*; △, $2.00 \cdot 10^{-4}$ *M*; ●, $4.00 \cdot 10^{-5}$ *M* anthraquinone-2,6-disulfonate.

rise with increasing residence time, and the curves for different AQDS concentrations lie in a sequential order, again indicating a proportionality between signal area and AQDS concentrations. For this reactor, the signal area has not yet reached an optimum, even for the longest reaction time. Reactor IV (8-W black lamp, 12-m knitted PTFE capillary) allows significantly longer residence times than reactor III, and the curves for the two higher AQDS concentrations reveal that similar mechanisms may take place at the longer residence times, as observed with reactors I and II at shorter residence times. The two curves for the lower AQDS concentrations demonstrate behavior similar to reactor III.

The improved signal areas resulting from longer reaction times under a low-flux lamp in comparison with shorter times under a high-flux lamp may be due to the kinetics of radical recombination[33]. A higher flux of photons generates a higher

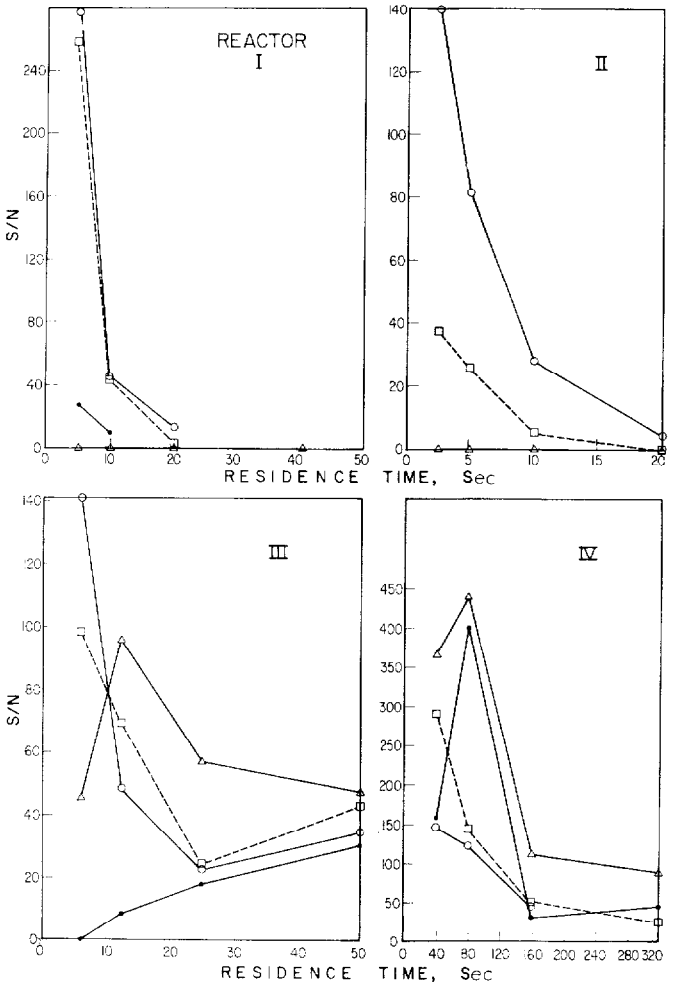

Fig. 8. Variation of S/N ratio with residence time in the photochemical reactor for various concentrations of anthraquinone-2,6-disulfonate. Single-pump detection scheme, C_8 column, Kontron fluorometer. ○, $1.20 \cdot 10^{-3}$ *M*; □, $6.00 \cdot 10^{-4}$ *M*; △, $2.00 \cdot 10^{-4}$ *M*; ●, $4.00 \cdot 10^{-5}$ *M* anthraquinone-2,6-disulfonate.

instantaneous concentration of radicals, and consequently radical termination reactions (disproportionation or combination) are much more favored. In other words, short-chainlength reaction mechanisms tend to occur. A lower flux produces lower instantaneous concentrations of radicals and longer-chainlength reaction mechanisms are favored. Although the mechanism desired, Fig. 1, has only four steps, it is possible that high instantaneous radical concentrations may favor some type of reaction (producing non-fluorescent products) between the initial radicals, α-hydroxyalkyl radical and the semiquinone, or more likely, between the initial radicals and the AQH_2DS. Consequently, it is likely that higher instantaneous radical concentrations favor reaction mechanisms that produce non-fluorescent products and possibly polymers.

The optimization of the S/N ratio, the most important criterion for analytical work, shown in Fig. 8, is consistent with the previously described results. In reactors I and II the S/N falls off much faster with increasing residence time than does the signal area itself. The decrease in S/N with increasing residence time is probably due to the combined effects of photodegradation of the fluorescent product and/or polymerization, the enlargement of the noise (produced by an increasing S_{bg} with increasing residence time), and the increased pump pulsations at longer residence times. The latter are due to a curtailment of the effectiveness in the pulse dampener at lower flow-rates, which produce a lower pressure drop. The S/N ratio for reactor III also falls off while the S_{area} continues to rise, and this effect is due entirely to the increased S_{bg} and the increased pump pulsations at lower flow-rates. In addition, since the capillary is made of Pyrex, an nonresilient material, very little pulse dampening will occur in this reactor. In the 1-m PTFE coil and especially in the 12.5-m PTFE knitted reactor, a significant amount of pulse dampening may occur. Finally, reactor IV shows behavior consistent with reactors I and II. At the two highest AQDS concentrations, the decrease in the S/N ratio with increasing residence time occurs as a result of photodegradation, rising S_{bg}, and increased pump pulsations. From Fig. 8, it is apparent that the highest S/N ratio is obtained with the small lamp, the knitted reactor coil, and an AQDS concentration of $2 \cdot 10^{-4}$ *M* and a residence time of 81 sec. Consequently, all analytical work was performed with photochemical reactor IV.

Band broadening

The only detrimental effect of coupling a post-column reactor to a HPLC column is the peak-broadening inside the reactor capillary and mixing units (if required). We chose to express this band-broadening in dispersion values, a manner often used in flow-injection analysis[36]. The dispersion is defined by

$$D = \frac{C^0}{C^{max}}$$

where C^0 is the concentration of the analyte without having undergone any band broadening, and C^{max} is the peak concentration of the analyte within a plug having undergone band broadening. Dispersion values for the four reactors were determined by injecting 15 μl of $1.00 \cdot 10^{-4}$ *M* salicylic acid to obtain a signal proportional to C^{max}. A signal proportional to C^0 was determined by injecting a 1-ml volume of the same solution.

TABLE I

DISPERSION OF PHOTOCHEMICAL REACTORS*

Flow-rate (ml/min)	*Reactor*				
	I	*II*	*III*	*IV*	*None*
2.0	5.45	5.42	7.24	6.14	5.23
1.0	4.12	3.39	6.62	4.15	2.91
0.5	3.37	2.88	4.80	4.27	2.18
0.25	2.89	2.54	4.36	6.30	1.87

* Expressed as $D = C^0/C^{max}$.

Table I compares the measured dispersion values for the various reactors at various flow-rates. It is no surprise that reactor II exhibits the lowest dispersion values, since it contains the least amount of PTFE tubing. Similarly reactor III has the largest dispersion values (except for the 0.25 ml/min flow-rate), because reactor III has the tubing with the largest I.D. Reactors I and IV demonstrate intermediate dispersion values, which are comparable at a flow-rate of 1 ml/min (the most commonly employed flow-rate), although reactor I has lower dispersion values at the other flow-rates. Additionally reactor IV exhibits a parabolic flow-rate *vs.* dispersion curve, completely different from the ascending flow-rate *vs.* dispersion curve of the

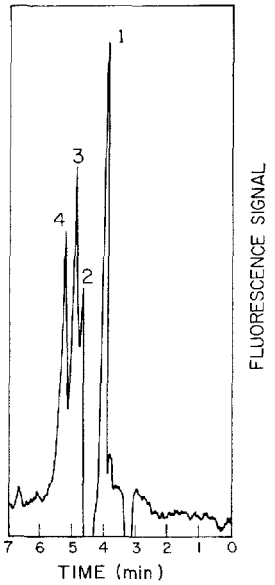

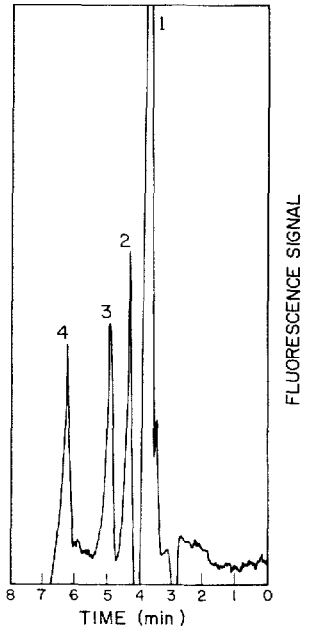

Fig. 9. Chromatogram of Class C cardiac glycosides. Peaks: 1 = solvent; 2 = 200 ng of digoxigenin; 3 = 200 ng of lanatoside C; 4 = 200 ng of digoxin. Single-pump detection scheme (Fig. 3). Flow-rate, 1 ml/min; residence time, 81 sec in Reactor IV; C_8 column; Kontron fluorometer.

Fig. 10. Chromatogram of various cardiac glycosides. Peaks: 1 = solvent; 2 = 200 ng of diginatin; 3 = 200 ng of digoxin; 4 = 200 ng of lanatoside B. Same experimental condition as Fig. 9.

coiled reactors. A similar phenomena was also observed by Uihlein and Schwab[16] and is most likely due to the type of velocity flow profile encountered in the intricate knitting pattern of the reactor.

Reproducibility

The reproducibility of the PRF detector was measured for the single pump scheme with the C_8 column and photochemical reactor IV. The measurement was made by comparing the peak heights of ten 15-μl injections containing 0.5 μg of diginatin. The relative standard deviation was 6.0%.

Chromatography

By adding the photochemical reagent (AQDS) to the mobile phase of the chromatographic apparatus, the separating power of reversed-phase and amino columns is greatly limited. In the past, we observed an improvement in the separation of small aliphatic alcohols, aldehydes, and ethers using a C_{18} column with a high percentage of acetonitrile[8]; however, the capacity factors, k', under these conditions are quite small, and this adds great difficulty to the analysis if the analytes are present in a matrix that contains a large peak due to unretained or weakly retained interfering compounds. Figs. 9 and 10 are chromatograms of a synthetic mixture of cardiac glycosides, while Fig. 11 is a chromatogram from an extract of a digoxin tablet. All three chromatograms were obtained with the single-pump detection scheme. We observed that *ca.* 40% acetonitrile gives the maximum retention, *i.e.*, k' values, whereas deviations from this concentration either way lower the retention times and k' values. This may be indicative of a mixed retention mechanism, an ion-exchange mechanism due to the AQDS and a reversed-phase mechanism from the reversed-phase ligands, since in reversed-phase chromatography an increase in retention would be expected in going from 40% acetonitrile to pure water.

A post-column addition scheme was constructed for the analysis of the saccharides since the addition of AQDS to the mobile phase of the amino column vitiated the separating power of the column. This detection scheme entailed two chromatographic columns and two pumps. The amino column was used to separate the saccharides, whereas the C_{18} column was employed to suppress the pulsations of the post-column addition pump. Since the C_{18} column, loaded with AQDS, does not retain the saccharides, almost no additional band broadening results from this column. Fig. 12 demonstrates the analysis of a soft drink by use of the dual pump scheme.

Detection limits

The detection limits for the cardiac glycosides and aglycones are near 40 ng (S/N = 3) with the exception of class A cardiac glycosides and aglycones. The class A glycosides and aglycones have only a tertiary hydroxy group on the steroid ring. Consequently, the steroid ring has only O–H bonds β and none α to the hydroxy group on the ring. Although the class A glycosides have primary and secondary hydroxy groups on their saccharide moieties, the saccharides have a lower response in comparison to less hydrophilic molecules. This lowered response to extremely hydrophilic molecules is thought to be due to the high amount of solvation which sterically hinders the hydrogen abstraction step[32]. For the remaining glycosides and

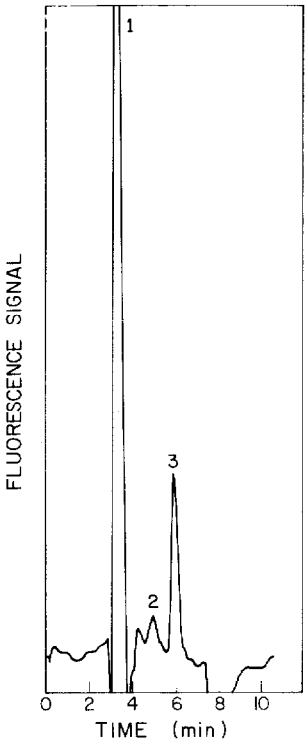

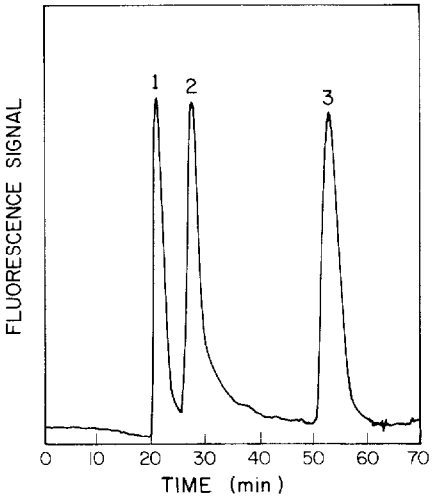

Fig. 11. Chromatogram of digoxin tablet. Peaks: 1 = lactose; 2 = impurity; 3 = 200 ng of digoxin. Single-pump detection scheme; C_{18} column; flow-rate, 1 ml/min; residence time, 81 sec in reactor IV; Schoeffel fluorometer.

Fig. 12. Chromatogram of a soft drink. Peaks: 1 = fructose; 2 = glucose; 3 = sucrose. Dual-pump detection scheme (Fig. 4); flow-rate, 1 ml/min for pre-column pump and 0.3 ml/min for post-column pump; Schoeffel fluorometer.

aglycones outside of Class A a linear working range of 50–500 ng was observed.

The detection limits (S/N = 3) for various common food saccharides —fructose, xylose, arabinose, glucose, maltose and lactose— were found to be *ca.* 0.4 μg when the dual-pump scheme with 60% acetonitrile was used. An additional reason, besides the increased amount of solvation for the detection limits of saccharides being higher than those of the cardiac glycosides and aliphatic alcohols, aldehydes, and ethers is that the dual-pump detection scheme introduced more noise than the single-pump detection scheme.

CONCLUSIONS

In this study, we have demonstrated a completely new type of detection system that does not require the analytes to absorb UV–visible radiation, or to fluoresce, or to be electrochemically active. Although we have not observed exceptionally low detection limits, we feel that the sensitivity of the PRF technique can only be judged in light of contemporary methods employed for the same types of determination. The

present sensitivity of the PRF detector for the cardiac glycosides and aglycones is not significantly better than the sensitivity obtained with 220 nm absorption. However, the PRF detector does demonstrate an improvement of one order of magnitude over the RI detector for the determination of saccharides. Furthermore, since the PRF detector has a selectivity aspect which the RI detector and UV detector is lacking, the interpretation of complex chromatograms is facilitated, and as a result, the determination of an analyte which responds to the PRF detector is greatly facilitated within a complex matrix. Consequently, if the sensitivity of the PRF detector could be improved, this type of detection scheme could prove quite valuable for determinations of many non-absorbing analytes in LC.

Presently, we are attempting to improve the detection limits of the PRF detector in two ways. First, we are trying to find a sensitizer with a much lower background signal, since a lowering of the background signal in the PRF system could entail a substantial improvement in the detection limits. Second, we are attempting to purify the solvents used in the HPLC mobile phase, as the background might be due to impurities such as amines in the acetonitrile.

ACKNOWLEDGEMENT

The authors gratefully acknowledge the support of the National Science Foundation (Grant No. CHE-7915801) and for a visitors grant to J.W.B. by Z.W.O. in Den Haag, The Netherlands. We are especially thankful to Jan Donkerbroek, Cees Gooijer, Tad Koch, Luboš Nondek, Cor de Ruiter, Gerrit de Vries and Ken Sigvardson for helpful discussions. Additionally, we wish to thank Pinus Walinga, Dick van Iperen, and Robert Kordes for their technical assistance in the construction of the photochemical reactors. Thanks are also due to Sandoz (Basle, Switzerland) for supplying the cardiac glycosides. Finally, we are greatly indebted to Karen Birks for knitting the photochemical reactor.

REFERENCES

1 R. W. Frei, in R. W. Frei and J. F. Lawrence (Editors), *Chemical Derivatization in Analytical Chemistry*, Vol. 1, Plenum, New York, 1981, pp. 211–340.
2 R. W. Frei and A. H. M. T. Scholten, *J. Chromatogr. Sci.*, 17 (1979) 152.
3 R. S. Deelder, M. G. F. Kroll, A. J. B. Beeren and J. H. M. Van Den Berg, *J. Chromatogr.*, 149 (1978) 669.
4 R. W. Frei, *Chromatographia*, 15 (1982) 161.
5 J. W. Birks and R. W. Frei, *Trends Anal. Chem.*, 1 (1982) 361.
6 W. Iwaoka and S. R. Tannenbaum, *IARC Sci. Publ.*, 14 (1976) 51.
7 D. J. Popvich, J. B. Dixon and B. J. Ehrlich, *J. Chromatogr. Sci.*, 17 (1979) 643.
8 M. S. Gandelman and J. W. Birks, *J. Chromatogr.*, 242 (1982) 21.
9 P. J. Twitchett, P. L. Williams and A. C. Moffat, *J. Chromatogr.*, 149 (1978) 683.
10 A. Bowd, D. A. Swann and J. H. Turnbull, *Chem. Commun.*, (1975) 797.
11 P. J. Harman, G. L. Blackman and G. Phillipou, *J. Chromatogr.*, 225 (1981) 131.
12 A. T. Rhys Williams, S. A. Winfield and R. C. Belloli, *J. Chromatogr.*, 235 (1982) 461.
13 A. H. M. T. Scholten, U. A. T. Brinkman and R. W. Frei, *Anal. Chim. Acta.*, 114 (1980) 137.
14 A. H. M. T. Scholten, P. L. M. Welling, U. A. T. Brinkman and R. W. Frei, *J. Chromatogr.*, 199 (1980) 239.
15 U. A. T. Brinkman, P. L. M. Welling, G. de Vries, A. H. M. T. Scholten and R. W. Frei, *J. Chromatogr.*, 217 (1981) 463.

16 M. Uihlein and E. Schwab, *Chromatographia*, 15 (1982) 140.
17 M. F. Lefevere, R. W. Frei, A. H. M. T. Scholten and U. A. T. Brinkman, *Chromatographia*, 15 (1982) 459.
18 A. H. M. T. Scholten, U. A. T. Brinkman and R. W. Frei, *J. Chromatogr.*, 205 (1981) 229.
19 M. S. Gandelman and J. W. Birks, *Anal. Chem.*, 54 (1982) 2131.
20 N. J. Turro, *Modern Molecular Photochemistry*, Benjamin/Cummings, Menlo Park, CA, 1978.
21 N. K. Bridge and G. Porter, *Proc. Roy. Soc., London, Ser. A*, 244 (1958) 259.
22 N. K. Bridge and G. Porter, *Proc. Roy. Soc., London, Ser. A*, 244 (1958) 276.
23 J. Rennert, S. Japar and M. Guttman, *Photochem. Photobiol.*, 6 (1967) 485.
24 F. Wilkinson, *J. Phys. Chem.*, 66 (1962) 2569.
25 K. Tickle and F. Wilkinson, *Trans. Faraday Soc.*, 61 (1965) 1981.
26 J. Beutel, R. J. Ruszkay and J. F. Brennan, *J. Phys. Chem.*, 73 (1969) 3240.
27 A. Ledwith, G. Ndaalio and A. R. Taylor, *Macromolecules*, 8 (1975) 1.
28 J. Rennert and P. Ginsberg, *J. Photochem.*, 4 (1975) 171.
29 A. Harriman and A. Mills, *Photochem. Photobiol.*, 33 (1981) 619.
30 J. L. Bolland and H. R. Cooper, *Proc. Roy. Soc., London, Ser. A*, 225 (1954) 405.
31 C. F. Wells, *Trans. Faraday Soc.*, 57 (1961) 1703.
32 C. F. Wells, *Trans. Faraday Soc.*, 57 (1961) 1719.
33 D. C. Nonhebel, J. M. Tedder and J. C. Walton, *Radicals*, Cambridge University Press, Cambridge, 1979.
34 K. P. Clark and H. I. Stonehill, *Trans. Faraday Soc. I*, 68 (1972) 578.
35 K. P. Clark and H. I. Stonehill, *Trans. Faraday Soc. I.*, 68 (1972) 1676.
36 J. Ruzicka and E. H. Hansen, *Flow Injection Analysis*, Wiley, New York, 1981, p. 16.